Optimised screw pile design for offshore jacket foundations in medium-dense sand

Cerfontaine, Benjamin; Brown, Michael; Davidson, Craig; Sharif, Yaseen; Huisman, Marco; Ottolini, Marius

Published in:
Geotechnique Letters

DOI:
10.1680/jgele.21.00105

Publication date:
2022

Optimised screw pile design for offshore jacket foundations in medium-dense sand

Cerfontaine, B., Brown, M.J., Davidson, C., Sharif, Y.U., Huisman, M., Ottolini, M.

Abstract: Screw piles are well suited foundations for offshore jacket structures, as they can be installed without significant underwater noise and have a large axial capacity. However, installation requirements for such large piles must be reduced to enable their installation in the field. This work combines geometry and installation optimisation to lower force and torque installation requirements. An original pile geometry, composed of a large diameter upper section connected to a smaller diameter lower section by a transition piece, was tested in a geotechnical beam centrifuge. The advancement ratio (AR), describing the relative vertical movement per pile rotation, was varied below the threshold usually recommended. Results show that a low AR reduces the pile penetration resistance and even generates some pull-in, while the torque remains almost unaffected. The torque is mainly associated with the upper section of the pile, which has a greater diameter to resist lateral loading in service. The pile capacity in tension generally increases as AR is reduced and reaches a maximum for AR = 0.5, while the compressive capacity reduces. It was shown that a simplified method can be used to estimate pile capacity, providing that some AR dependent reduction factors can be calculated or assumed.

Keywords: Offshore engineering, Anchors & anchorages, Centrifuge modelling, sand

1. Introduction

Screw (or helical) piles are a “silent” installation alternative to pile driving for offshore foundations (Spagnoli and Tsuha, 2020). Typical onshore geometries consist of a long shaft connected to several deeply embedded helices to enhance axial capacity (Perko, 2009). Screw pile lateral capacity is dominated by the shaft (or core) behaviour, with helices providing extra resistance (Al-Baghdadi *et al.*, 2017; Kwon *et al.*, 2019). However, increasing the shaft diameter or number of helices to meet offshore foundation needs creates greater installation requirements, i.e. installation torque and penetration resistance (Davidson *et al.*, 2020), which may not be easily applied by current installation vessels.

The advancement ratio (AR) is defined as the ratio between the vertical displacement of the pile per one rotation (Δz_h) divided by the helix pitch (p_h) (Bradshaw *et al.*, 2018)

$$AR = \frac{\Delta z_h}{p_h} \quad (1)$$

Standards recommend that this ratio varies within 1±0.15 during installation (BS8004:2015, 2015), which is termed pitch-matched. It was shown experimentally (Cerfontaine *et al.*, 2021a) and numerically (Sharif *et al.*, 2021b) that relaxing this constraint in sands (AR $\leq$0.85, termed pile overflighting) considerably reduces the vertical force necessary for installation.

Jacket structures supporting offshore wind turbine impose large axial and lateral loads to their foundations. A large screw pile shaft diameter would be necessary to resist those loads, which increases the pile penetration resistance (Davidson *et al.*, 2020). The objective of this work is to demonstrate that geometry and installation processes can be optimised to ensure the feasibility of screw piles. Centrifuge modelling of an original design, combining one helix, two shaft diameters and a bespoke transition piece, was undertaken to show the AR effect on installation requirements and resistance in both tension and compression.

2. Experimental set-up

Two 3D printed stainless steel closed-ended screw pile models were tested in the geotechnical beam centrifuge at the University of Dundee (UK). Each model (see Table 1 for dimensions) is composed of lower and upper sections connected via a transition piece, while a helix is attached to the lower section (Figure 1). Two transition pieces were tested, a conical piece (named CTP, Figure 1b) and an internal helix (named IHTP, Figure 1a, D_h/p_h = 2.8). The internal helix, identical to the lower helix, enables the sand to enter the pile upper section in an attempt to reduce installation requirements. The model pile was connected to an actuator capable of installing and loading the pile in a single centrifuge flight (Al-Baghdadi, 2018; Davidson *et al.*, 2020). Whilst spinning at 62g, installation of the pile was undertaken by imposing a constant rotation rate (3RPM) and using different vertical installation rates to achieve the required AR (equal to $3 \cdot \mathrm{AR} \cdot \mathrm{p_h}$) until the target embedment depth (20m-30m at prototype scale) was reached. Tensile or compressive loading was then imposed at a constant vertical displacement rate (1mm/min) after a 5 minute resting period.

Medium-dense sand beds (43 m deep, average relative density 52%-57%) were created by dry pluviation of HST95 sand (properties in Table 2 (Al-Defae *et al.*, 2013; Robinson *et al.*, 2019)) in a strong box (500 mm x 800 mm x 550 mm). Tests were undertaken in dry sand at 62g, corresponding to a scale (N) 1:100 in an equivalent saturated sand behaving in a drained manner (Li *et al.*, 2010), which is the case here.

Further details regarding the testing rig, sample preparation and in-flight CPT can be found in Davidson *et al.* (2020). Fifteen tests were undertaken (Table 3), varying the pile geometry, embedment depth, advancement ratio and testing tensile or compressive resistance.

3. Results and discussion

Figure 2 shows installation requirements (vertical force in Figure 2a, torque in Figure 2b) as a function of the embedment depth, geometry and AR. Figure 2a shows that reducing the AR reduces the measured vertical force, from 21MN in compression (pitch-matched, AR = 1.0) to tension in the pile (overflighting, AR = 0.5). This behaviour is consistent with previous single

54 helix pile behaviour (Cerfontaine *et al.*, 2021a). It was shown numerically that helix overflighting
55 forces sand particles to move upwards (Cerfontaine *et al.*, 2021b). However, the surrounding
56 soil opposes this upwards movement and the reaction force acting on the helix creates tension
57 in the pile (pull-in force). When the pile upper section penetrates the soil (from 10.5m depth),
58 the pile penetration resistance increases due to the transition piece and larger shaft diameter,
59 even if the helix pull-in continues to increase.
60 It was measured that the internal helix opening plugged during the installation (final plug height
61 equal to 2.0m-2.5m). Plugging prevents the sand from entering the upper section. Therefore,
62 the transition pieces have different penetration mechanisms, similar to a CPT device (for CTP)
63 or to a cutting tool (for plugged IHTP). Figure 2a shows that penetration resistance of the CTP
64 is greater than the IHTP, as the measured force is more in compression (Figure 2a , AR = 0.5,
65 depth >10.5m). The torque is also lower for the IHTP (Figure 2b). The conical piece test was
66 repeated in two successive sand beds to demonstrate the reproducibility of the results.
67 This relative insensitivity of the measured torque to AR (Figure 2b) is beneficial for design and
68 application, as an error in the estimated or applied AR won't significantly affect the required
69 torque, and hence lead to early refusal. The torque started to increase more importantly after
70 the upper section penetrated (10.5m depth, Figure 2b), which can be related to a greater shaft
71 diameter (lever arm, increased surface area) and the transition piece. At the end of installation,
72 the torque varied between 21MNm and 24MNm for the IHTP, while the conical piece torque
73 was 27MNm. These values are lower than the maximum that was deemed practically
74 achievable with installation vessels.
75
76 Screw piles (with IHTP) were installed at AR ranging from 0.1 to 1.0 at a depth of 25m, then
77 tested in tension or compression. Representative load-displacement relationships are shown
78 in Figure 3. Capacity and initial stiffness of the pile tend to increase in tension as the AR
79 decreases, while the opposite effect can be observed in compression, which is consistent with
80 experimental and numerical results (Cerfontaine *et al.*, 2021a; Sharif *et al.*, 2021b). The
81 prediction of foundation initial stiffness is critical in the design of offshore wind turbines, which

82 are dynamically sensitive. It was shown by Jalbi *et al.* (2019), that high vertical stiffness for
83 jacket foundations is preferable to avoid low frequency rocking modes of vibration and
84 susceptibility to resonance with the rotor frequency. Therefore, the pile initial stiffness
85 enhancement due to overflighting is beneficial for design. This enhancement of capacity and
86 stiffness can again be explained by the overflighting movement of the helix, which enhances
87 soil density and the stress field above the helix and has the opposite effect underneath the
88 helix. The effect on the pile shafts was not measured, but it could be expected that overflighting
89 increases the radial stress magnitude, hence the shaft vertical resistance (Cerfontaine *et al.*,
90 2021b; Sharif *et al.*, 2021b). The pile behaviour only exhibits a well-defined peak in tension,
91 hence the pile resistance (denoted $F_{z,r}$) was calculated as the maximum force measured within
92 $0.1D_h$ displacement.
93 Figure 4 shows a continuously decreasing compressive capacity with reduction in AR, while
94 the tensile capacity of overflighted piles is always greater than the pitch-matched one, with a
95 maximum for AR = 0.5. Tensile capacity is critical for jacket supported wind turbines (Davidson
96 *et al.*, 2020). Therefore, the potential for tensile capacity increase with a reduction in AR will
97 be beneficial, while the reduction in compressive capacity wouldn't necessarily affect the
98 design. The torque at the end of installation is also reported in Figure 4, but does not show a
99 clear trend, although it is maximum for AR = 0.5. The small difference between installation
100 torques measured for tests at a same AR shows the good reproducibility of the results. The
101 pile capacity after overflighting installation (AR = 0.5) was measured at two additional
102 penetration depths (20m and 30m). Figure 5 depicts that the change in compressive or tensile
103 resistance from 20m to 30m depth is approximately twice the change in resistance due to AR
104 variations. Therefore, including AR dependence in the pile capacity calculation has the
105 potential to reduce the required pile penetration depth, hence the torque requirements saving
106 time and money.
107
108 The pile axial resistance is due to the (upper) shaft and lower helix in tension, while the
109 compressive capacity includes the transition piece contribution. The lower shaft contribution

can be ignored due to its relatively small diameter (D_{low}/D_h = 0.4), short length and interaction with the helix failure mechanisms (already included via Eq. (2)). Meyerhof and Adams (1968) postulated that the bearing factor (N_γ) for helix or plates in tension increases with depth (shallow failure mechanism) until a certain depth, after which the bearing factor is constant (deep failure mechanism). As a first approximation, the method proposed by Giampa *et al.* (2017) was used to calculate N_γ (shallow mechanism)

$$\frac{F_h}{\gamma' z A_h} = N_\gamma\left(\frac{z}{D_h}\right) = 1 + 2F_{ps}\left(\frac{z}{D_h}\right) + \frac{4}{3}F_{ps}\tan\psi_p\left(\frac{z}{D_h}\right)^2 \leq N_\gamma\left(\frac{z}{D_h} = 6\right) \quad (2)$$

where

$$F_{ps} = \tan\psi_p + \cos\left(\phi_p - \psi_p\right)\left(\tan\phi_p - \tan\psi_p\right) \quad (3)$$

and F_h is the helix capacity, ϕ_p is the soil peak friction angle (see Table 2), ψ_p is the peak dilatancy angle, γ' is the effective unit weight and A_h is the helix area. The deep bearing factor was calculated by assuming the shallow to deep transition takes place at a relative depth around $z/D_h = 6$ in medium-dense HST95 sand (Cerfontaine *et al.*, 2019). Bearing factors are potentially greater in compression than in tension (Lutenegger and Tsuha, 2015), but they were considered identical here as there were no measurements available to determine the helix contribution.

The upper shaft and transition piece contributions can be estimated based on the method proposed by Lehane *et al.* (2007) for jacked piles. The compressive capacity of the transition piece, considered as a fully plugged tip is

$$F_{tp} = 0.6\bar{q}_c\frac{\pi}{4}D_{up}^2 \quad (4)$$

where D_{up} is the diameter of the upper section shaft and $\bar{q}_c$ is the averaged cone penetration resistance, extrapolated from (Davidson *et al.*, 2020). The shaft contribution is calculated by integrating numerically the shear stress along the embedment depth

$$\tau_f = a\ \bar{q}_c \left[\max\left(\frac{h}{D_{up}}, 2\right)\right]^{-0.5} \tan\delta_{crit} \quad (5)$$

where a is a drop index equal to 0.03 in compression and 0.022 in tension, h is the distance measured upwards from the base of the transition piece and δ_{crit} is the interface friction angle.

The prediction of pile axial capacity is depicted in Figure 5 as a dashed line, which is consistent with pitch-matched installation (AR = 1.0) at 25m depth. Using results from Figure 4, it is possible to calculate an AR based reduction factor (f_{AR}) to correct the results (solid line in Figure 5), which better approximates the centrifuge results (AR = 0.5). The proposed method gives an estimate for pile resistance, but more results are necessary to determine accurate AR correction factors. Firstly, pile jacking or helical pile embedment leads to different mechanisms during installation (see Cerfontaine *et al.* (2021b)). Secondly, the AR effect on the helix or the shaft resistances are probably different and function of many parameters, such as the embedment depth and pile and helix geometric properties.

Future research is necessary to determine correction factors for each contribution (shaft, helix, transition piece) and to optimise the transition piece to reduce installation torque. The use of DEM to investigate local mechanisms during installation (Cerfontaine *et al.*, 2021b) or loading (Sharif *et al.*, 2021b, 2021a) of screw piles can be used to enrich experimental findings and develop physically-based prediction methods. Finally, installation in the field will be undertaken at constant vertical force (pile and tool weight), with the AR adapting to maintain the vertical equilibrium. The effect of this mode of installation on the capacity needs further investigation.

4. Conclusions

An original screw pile design, composed of two parts of varying shaft diameter, was tested in a geotechnical centrifuge. It was shown that their penetration resistance can be reduced by geometry and installation optimisation, which enables their use as foundations for jacket structures supporting offshore wind turbines and minimises the reaction forces needed from

installation vessels. It was shown that reducing the advancement ratio during pile installation strongly reduces the need for vertical reaction force, while the required torque was relatively unchanged. The torque appears to be mostly due to the upper pile section, whose length and transition piece should be optimised to reduce installation requirements, with the IHTP having the lowest penetration resistance. The tensile resistance was always smaller than the compressive capacity, but the tensile capacity increased with a reduction of AR, while the compressive capacity decreased. An estimation method was proposed to calculate the pile capacity in both tension and compression. Predictions were consistent with the capacities measured experimentally, but more research is needed to derive AR-dependent correction factors.

5. Acknowledgements

The authors would like to acknowledge the support of the Engineering and Physical Science Research Council (EPSRC) (Grant no. EP/N006054/1: Supergen Wind Hub Grand Challenges Project: Screw piles for wind energy foundations).

6. Notation

a	Stress drop index, from (Lehane *et al.*, 2007)
A_h	Helix surface (including shaft)
AR	Advancement ratio
D_h	Helix diameter
D_{low}	Diameter of the screw pile lower shaft
D_r	Relative density
D_s	Shaft diameter
D_{up}	Diameter of the screw pile upper shaft

F_h	Resultant force acting on the helix
F_s	Resultant force acting on the shaft
F_{tp}	Resultant force acting on transition piece
F_z	Total vertical force
$F_{z,r}$	Total vertical force at failure (within $0.1D_h$) in tension or compression
L_{up}	Length of the lower section shaft
L_{up}	Length of the upper section shaft
N_γ	Helix non-dimensional bearing factor
p_h	Helix pitch
$\bar{q}_c$	Averaged cone penetration resistance
t_p	Helix plate thickness
T	Total torque
z	Depth
α	Angle of the conical transition piece, to the vertical direction
γ'	Buoyant unit weight (=dry weight in this study)
δ_{crit}	Critical state interface friction angle
Δz_h	Vertical displacement of the helix after one helix revolution
τ_z	Vertical shear stress

7. References

Al-Baghdadi, T. (2018) *Screw piles as offshore foundations : Numerical and physical modelling. PhD thesis.* University of Dundee, UK.

Al-Baghdadi, T. A., Brown, M. J., Knappett, J. A. and Al-Defae, A. H. (2017) Geotechnical engineering effects of vertical loading on lateral screw pile performance, *Proceedings of the Institution of Civil Engineers: Geotechnical Engineering*, 170(3), pp. 259–272. doi: 10.1680/jgeen.16.00114.

Al-Defae, A. H., Caucis, K. and Knappett, J. A. A. (2013) Aftershocks and the whole-life seismic performance of granular slopes, *Géotechnique*, 63(14), pp. 1230–1244. doi: 10.1680/geot.12.P.149.

Bradshaw, A. S., Zuelke, R., Hildebrandt, L., Robertson, T. and Mandujano, R. (2018) Physical modelling of a helical pile installed in sand under constant crowd, in Davidson, C., Knappett, J. A., Brown, M. J., Brennan, A. J., Augarde, C., Coombs, W., Wang, L., Richards, D., White, D., and Blake, A. (eds) *Proceedings of the 1st International Symposium on Screw Piles for Energy Applications (ISSPEA)*. Dundee, UK, pp. 109–115. doi: https://doi.org/10.20933/100001123.

BS8004:2015 (2015) Code of practice for foundations. BSI Standards Limited.

Cerfontaine, B., Brown, M. J., Knappett, J. A., Davidson, C., Sharif, Y. U., Huisman, M., Ottolini, M. and Ball, J. D. (2021a) Control of screw pile installation to optimise performance for offshore energy applications, *Géotechnique (Ahead of Print)*. doi: 10.1680/jgeot.21.00118.

Cerfontaine, B., Ciantia, M. O., Brown, M. J. and Sharif, Y. U. (2021b) DEM study of particle scale and penetration rate on the installation mechanisms of screw piles in sand, *Computers and Geotechnics*. doi: 10.1016/j.compgeo.2021.104380.

Cerfontaine, B., Knappett, J. A., Brown, M. J. and Bradshaw, A. S. (2019) Effect of soil deformability on the failure mechanism of shallow plate or screw anchors in sand, *Computers and Geotechnics*, 109. doi: 10.1016/j.compgeo.2019.01.007.

Davidson, C., Brown, M. J. M. J. M. J., Cerfontaine, B., Al-Baghdadi, T., Knappett, J., Brennan, A., Augarde, C., Coombs, W., Wang, L., Blake, A., Richards, D. and Ball, J. D. (2020) Physical modelling to demonstrate the feasibility of screw piles for offshore jacket supported wind energy structures, *Géotechnique*, pp. 1–19. doi: 10.1680/jgeot.18.p.311.

Giampa, J. R., Bradshaw, A. S. and Schneider, J. A. (2017) Influence of Dilation Angle on Drained Shallow Circular Anchor Uplift Capacity, *International Journal of Geomechanics*, 17(2), p. 4016056. doi: 10.1061/(ASCE)GM.1943-5622.0000725.

209 Jalbi, S., Nikitas, G., Bhattacharya, S. and Alexander, N. (2019) Dynamic design
210 considerations for offshore wind turbine jackets supported on multiple foundations, *Marine*
211 *Structures*. Elsevier Ltd, 67(September 2018), p. 102631. doi:
212 10.1016/j.marstruc.2019.05.009.

213 Kwon, O., Lee, J., Kim, G., Kim, I. and Lee, J. (2019) Investigation of pullout load capacity for
214 helical anchors subjected to inclined loading conditions using coupled Eulerian-Lagrangian
215 analyses, *Computers and Geotechnics*. Elsevier, 111(March), pp. 66–75. doi:
216 10.1016/j.compgeo.2019.03.007.

217 Lauder, K. (2010) *The performance of pipeline ploughs*. PhD thesis, University of Dundee, UK.

218 Lehane, B. M., Schneider, J. A. and Xu, X. (2007) Development of the UWA-05 design method
219 for open and closed ended driven piles in siliceous sand, *Geotechnical Special Publication*,
220 40902(158), pp. 1–10. doi: 10.1061/40902(221)12.

221 Lehane, B., Schneider, J. and Xu, X. (2005) The UWA-05 method for prediction of axial
222 capacity of driven piles in sand, in Gourvenec, S. and Cassidy, M. (eds) *Frontiers in Offshore*
223 *Geotechnics: ISFOG*. Perth, Asutralia, pp. 683–689. doi: 10.1201/noe0415390637.ch76.

224 Li, Z., Haigh, S. K. and Bolton, M. D. (2010) Centrifuge modelling of mono-pile under cyclic
225 lateral loads, in *Proceedings of the 7th International Conference on Physical Modelling in*
226 *Geotechnics*, pp. 965–970. doi: 10.1680/ijpmg.2010.10.2.47.

227 Lutenegger, A. J. and Tsuha, C. H. C. (2015) Evaluating installation disturbance from helical
228 piles and anchors using compression and tension tests, *Proceedings of the 15th Pan-American*
229 *Conference on Soil Mechanics and Geotechnical Engineering*, (November), pp. 373–381. doi:
230 10.3233/978-1-61499-603-3-373.

231 Meyerhof, G. G. and Adams, J. I. (1968) The ultimate uplift capacity of foundations, *Canadian*
232 *Geotechnical Journal*, 5(4), pp. 225–244. Available at: papers3://publication/uuid/3BDC6C97-
233 03BC-4333-908A-C3CC077F995F.

234 Perko, H. A. (2009) *Helical Piles. A practical guide to design and installation*. 1st Ed. John

235 Wiley & Sons, Inc. doi: 10.1002/9780470549063.

236 Robinson, S., Brown, M. J., Matsui, H., Brennan, A., Augarde, C., Coombs, W. and Cortis, M.
237 (2019) Centrifuge testing to verify scaling of offshore pipeline ploughs, *International Journal of*
238 *Physical Modelling in Geotechnics*, 19(6), pp. 305–317. doi: 10.1680/jphmg.17.00075.

239 Sharif, Y., Brown, M. J., Ciantia, M., Cerfontaine, B., Davidson, C. and Knappett, J. (2021a)
240 Assessing single helix screw pile geometry on offshore installation and axial capacity.,
241 *Proceedings of the Institution of Civil Engineers - Geotechnical Engineering*, 175(5), pp. 512–
242 529. doi: 10.1680/jgeen.21.00104.

243 Sharif, Y. U., Brown, M. J., Cerfontaine, B., Davidson, C., Ciantia, M., Knappett, J., Brennan,
244 A., Ball, J. D., Augarde, C., Coombs, W., Blake, A., Richards, D., White, D., Huisman, M. and
245 Ottolini, M. (2021b) Effects of screw pile installation on installation requirements and in-service
246 performance using the Discrete Element Method, *Canadian Geotechnical Journal*, 58(9), pp.
247 1334–1350. doi: 10.1139/cgj-2020-0241.

248 Spagnoli, G. and Tsuha, C. H. C. (2020) A review on the behavior of helical piles as a potential
249 offshore foundation system, *Marine Georesources & Geotechnology*. Taylor & Francis, 0(0),
250 pp. 1–24. doi: 10.1080/1064119X.2020.1729905.

251 Wind Europe. 2018. Offshore wind in Europe. *In* Offshore Wind in Europe: key trends and
252 statistics 2017. doi:10.1016/S1471-0846(02)80021-X.

8. Caption list: figures

Figure 1 Screw pile models used in the centrifuge and main geometric parameters. (a) Internal helix transition piece; (b) Conical transition piece.

Figure 2 Representative installation (a) vertical force (F_y) and (b) Torque, as a function of depth, of the imposed AR and of the pile geometry.

Figure 3 Load-displacement relationship in tension or compression for piles embedded at 25m depth, as a function of the advancement ratio (AR)

Figure 4 Change in pile tensile or compressive capacity and change of torque at the end of installation as a function of the advancement ratio. Pile capacity is calculated as the maximum value within $0.1D_h$ displacement from the end of installation (25m depth at prototype scale).

Figure 5 Evolution of the pile capacity in tension (T) or compression (C) as a function of embedment depth for AR =0.5 and prediction via a simplified approach. The horizontal lines indicate the range of variation of measured pile resistance as a function of the AR.

9. Figures

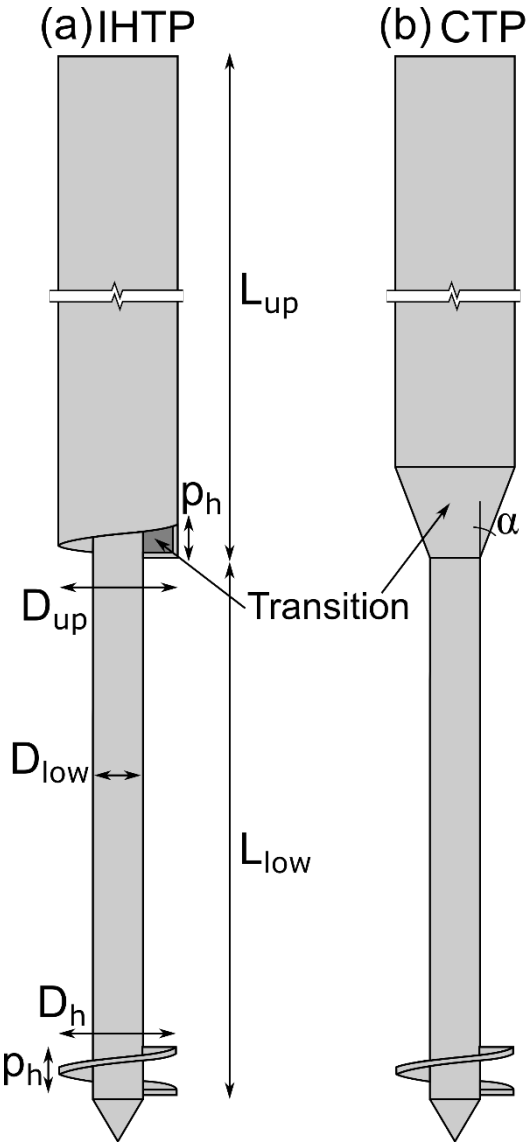

Figure 1 Screw pile models used in the centrifuge and main geometric parameters. (a) Internal helix transition piece (IHTP); (b) Conical transition piece (CTP).

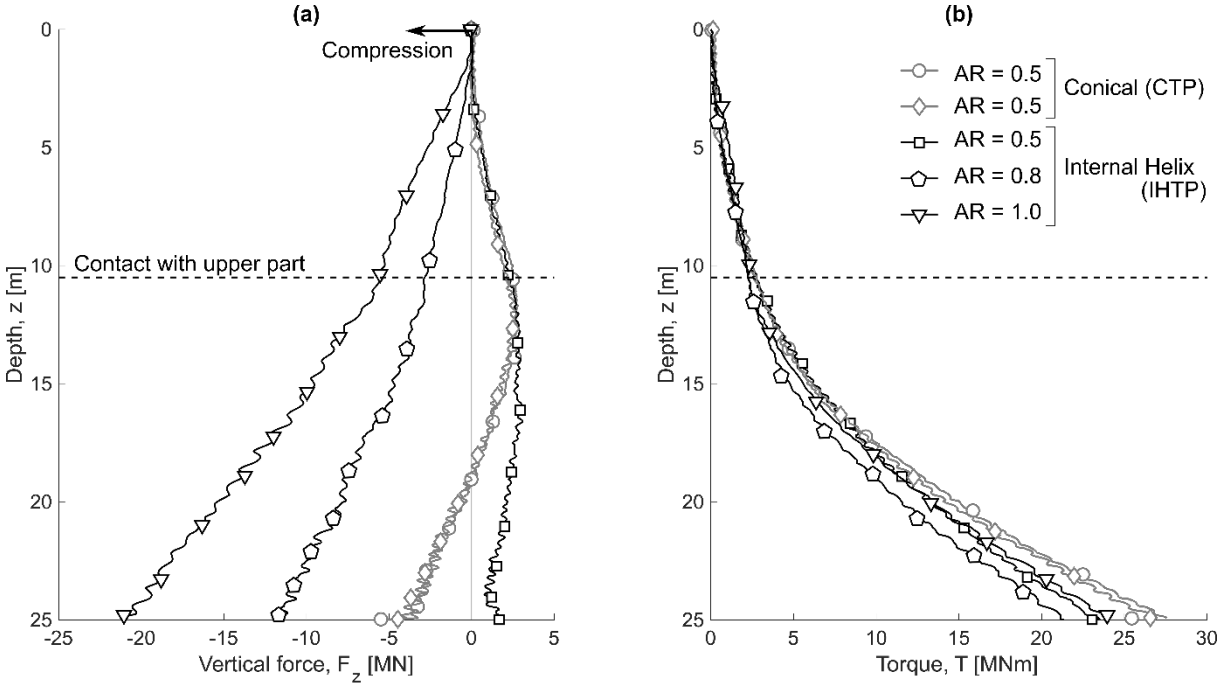

Figure 2 Representative installation (a) Vertical force (F_y) and (b) Torque, as a function of depth, of the imposed AR and of the pile geometry (conical transition piece CTP or internal helix transition piece IHTP). Test IDs: 1-3, 7, 10.

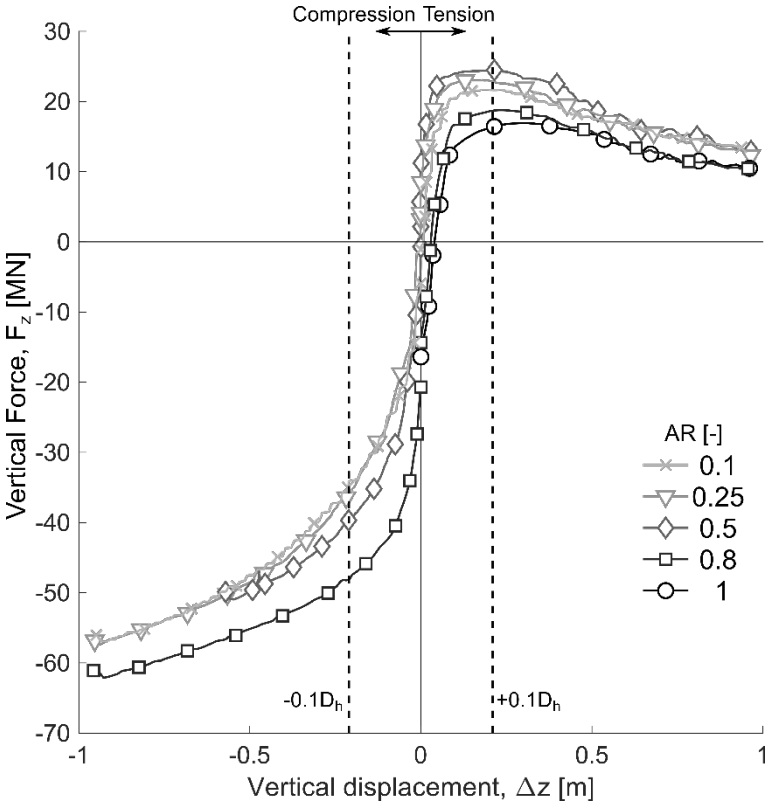

Figure 3 Load-displacement relationship in tension or compression for piles embedded at 25m depth, as a function of the advancement ratio (AR). Test IDs: 2, 4-7, 9-12.

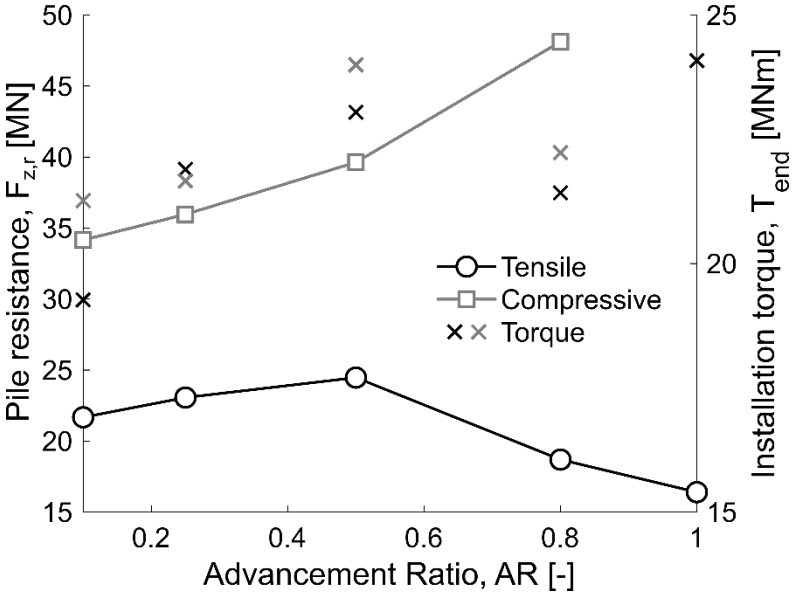

Figure 4 Change in pile tensile or compressive capacity and change of torque at the end of installation as a function of the advancement ratio (cross markers, one for compressive – grey – and one for tensile – black – tests). Pile capacity is calculated as the maximum value within $0.1D_h$ displacement from the end of installation (25m depth at prototype scale). Test IDs 2, 4-7, 9-12.

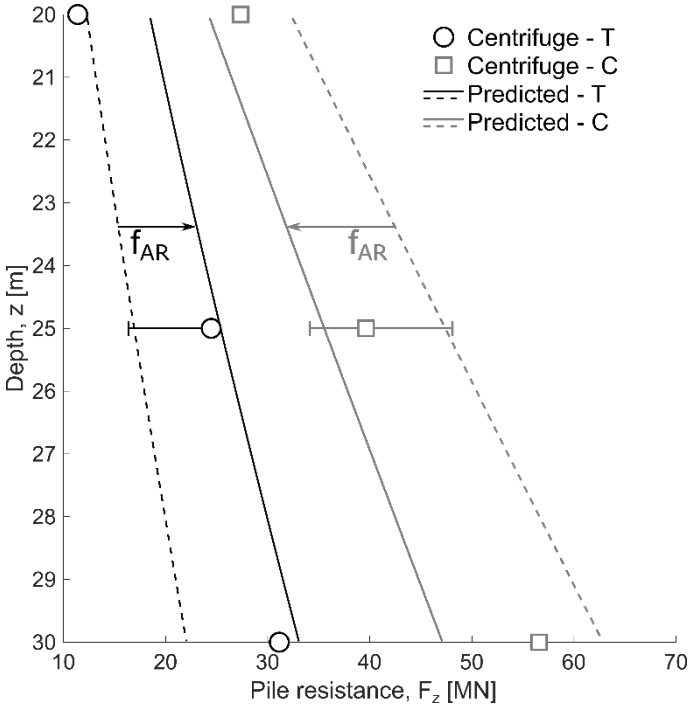

Figure 5 Evolution of the pile capacity in tension (T) or compression (C) as a function of embedment depth for AR =0.5 and prediction via a simplified approach. Correction factors $f_{AR} = 0.75$ in compression and $f_{AR} = 1.5$ in tension are applied from pitch-matched (AR = 1.0, solid lines) to overflighted (AR=0.5, dashed lines) predictions. The horizontal lines indicate the range of variation of measured pile resistance as a function of the AR. Test IDs: 2, 5, 8, 13-15.

10. Caption list: tables

Table 1 Properties of the HST95 sand, after (Lauder, 2010; Al-Defae *et al.*, 2013), peak friction angle given at 53% relative density

Table 2 Parameters of the pile at prototype scale

Table 3 List of centrifuge tests undertaken, average relative density of the sand bed (Dr), Imposed Advancement Ratio (AR), Target installation depth at prototype scale and loading test type (tensile T or compressive C)

11. Tables

Table 1 Parameters of the pile at prototype scale

Parameter	Symbol	Unit	Value
Upper section length	L_{up}	[m]	27.5
Lower section length	L_{low}	[m]	10.5
Upper section diameter	D_{up}	[m]	2.1
Upper section inner diameter	$D_{up,in}$	[m]	1.9
Lower section diameter	D_{low}	[m]	0.87
Helix diameter	D_h	[m]	2.1
Helix pitch	p_h	[m]	0.75
Helix plate thickness	t_p	[m]	0.1
Conical transition angle	α	[°]	40

Table 2 Properties of the HST95 sand, after (Lauder, 2010; Al-Defae *et al.*, 2013), peak friction and dilatancy angles given at 53% relative density (triaxial test). Interface friction was determined by direct shear test.

Parameter	Symbol	Unit	Value
Effective particle size	D_{10}	[mm]	0.09
Average particle size	D_{50}	[mm]	0.14
Particle specific gravity	G_s	[-]	2.63
Minimum void ratio	e_{min}	[-]	0.467
Maximum void ratio	e_{max}	[-]	0.769
Minimum dry density	ρ_{min}	[kg/m³]	1486
Maximum dry density	ρ_{max}	[kg/m³]	1793
Critical state friction angle	ϕ_{crit}	[°]	32
Peak friction angle	ϕ_p	[°]	39.6
Peak dilatancy angle	ψ_p	[°]	9.2
Sand-steel interface friction angle	δ_{crit}	[°]	24

Table 3 List of centrifuge tests undertaken, average relative density of the sand bed (D_r), Imposed Advancement Ratio (AR), Target installation depth of the tip at prototype scale and loading test type (tensile T or compressive C)

ID	Transition Piece	D_r [%]	AR [-]	Depth [m]	ULS
1	Conical	57	0.5	25	T
2	Internal Helix	57	0.5	25	T
3	Conical	52	0.5	25	T
4	Internal Helix	53	0.25	25	T
5	Internal Helix	52	0.5	25	C
6	Internal Helix	52	0.25	25	C
7	Internal Helix	52	1.0	25	T
8	Internal Helix	52	0.5	20	T
9	Internal Helix	52	0.1	25	T
10	Internal Helix	52	0.8	25	T
11	Internal Helix	54	0.1	25	C
12	Internal Helix	54	0.8	25	C
13	Internal Helix	54	0.5	20	C
14	Internal Helix	54	0.5	30	C
15	Internal Helix	52	0.5	30	T